THE PHENOMENON OF WAKES FORMATION AND DEVELOPMENT BEHIND LIQUID DROPLETS

Waheed, M. A.

Mechanical Engineering Department,
Ladoke Akintola University of Technology
P. M. B. 4000, Ogbomoso, Nigeria

ABSTRACT

Numerical simulations of spherical droplets sedimenting in a Newtonian fluid in an unbounded region were investigated by using finite element method for Reynolds number up to 300. The computations are thereby carried out with the penalty method instead of the integral method. The effect of the viscosity ratio η^* in the range $0.02 < \eta^* < 1000$ and the density ratio ρ^* in the range $0.02 < \rho^* < 1000$ on the wake formation and development was studied. It was observed that no wake is formed behind a droplet when the viscosity ratio η^* is below 2.3. The critical Reynolds number for a droplet with fluid properties $\rho^* = 1$ and $\eta^* = 50$ and another droplet with fluid properties $\rho^* = 1000$ and $\eta^* = 50$ is the same, and is 28.5. The viscosity ratio thus has strong effect on wake formation while density ratio has an insignificant effect. Further results show that the wake length and the angle of separation depend very strongly on the viscosity ratio. The results are very useful for the design and optimisation of engineering equipment where droplets occur.

Key words: Droplet, Two-phase Flow, Stream Function, Streamline, Viscosity Ratio, Wake

Nomenclature

A	Area of projection of a droplet, (m²)
C_D	Drag coefficient
d_d	Diameter of the droplet, (m)
F	Total drag force, (N)
$\mathbf{F}$	Matrix for the boundary conditions
g	Acceleration due to gravity, (m/s²)
L^1	Continuity matrix
M_p	Pressure matrix
$N(u)$	Matrix of the discretised convective term
p	Pressure, (N/m²)
r	Horizontal coordinate
R	Radius of the drop, (m)
Re	Reynolds number
S	Dissipation matrix
u	Vector of unknown velocities u_r and u_z, (m/s)
u_r	Horizontal velocity, (m/s)
u_z	Vertical velocity, (m/s)
u_∞	Velocity at infinitely far distance from droplet, (m/s)
z	Vertical coordinate

Greek Symbols

δ	Residual or error
τ	Penalty parameter
η_c	Viscosity of the continuous phase, (Pas)
η_d	Viscosity of the dispersed phase, (Pas)
$\eta^* = \eta_d / \eta_c$	Viscosity ratio
ρ_c	Density of the continuous phase, (kg/m³)
ρ_d	Density of the dispersed phase, (kg/m³)
$\rho^* = \rho_d / \rho_c$	Density ratio
ψ	Stream function, (m³/s)
Ω	Solution domain

INTRODUCTION

Droplet is a basic object in industrial processes. It occurs in many modern technologies such as in carburation as a prelude to combustion, ink jet printing, spray drying, net shape forming, in ore treatment (flotation), in biotechnology (inverse fluidised-bed bioreactor), and in micro-encapsulation and manufacturing. It has thus become the object of research for many engineers and scientists in the past few decades. In the past, the fluid dynamics of solid sphere has been extensively investigated. Examples of published works on flow over solid spheres are those by Lin and Lee (1973), Pruppacher et al. (1970), and Taneda (1956). Investigation of the viscous flow past liquid droplets has gained increase attention. Published works on fluid dynamics of liquid droplets include those by Feng and Michaelides (2001), El-Shaarawi et al. (1997), Wham et al. (1997), and Frohn and Roth (2000). The increase research work on droplet is due to the fact that a thorough knowledge of the fluid flow in and around a liquid droplet is of central importance to the study of heat and mass transfer between the droplets and the surrounding phase. The designs and the optimisation of engineering equipment involving fluid flow, heat and mass transfer have been done in the past by relying purely on both experimental and theoretical methods. But the theoretical analysis of the dynamics of droplets has been limited to creeping (Hadamard, 1911, Rybczynski, 1911), potential and boundary-layer flows (Chao, 1962), while the experimental work on single droplet seem almost impossible due to its small size (Sirignanoi, 1993). The most seemingly fruitful solution approach to the intermediate flow regime of the system is that based on numerical computation. The past works on the two-phase flow between a single droplet and the continuous phase system have concerned themselves with the computation of the drag force and coefficient for gas bubble, solid sphere and also to very limited cases for the liquid droplets with very high ratio of the viscosity between the droplet and the continuous phase η^*, e. g. water droplet in air (Sirignanoi, 1993; Brander and Brauer, 1993; Oliver and Chung, 1985).

While wake formation behind a solid sphere has been investigated extensively (Taneda, 1956), the phenomenon of wake formation and development behind a droplet has not been thoroughly studied. Wakes formation behind a droplet has been attributed to the effect of mass transfer process between it and the surrounding or as a result of fluid flow (Garner and Tayeban, 1960).

The present work is concerned with the investigation of the effect of the fluid properties on the wake formation and development. The effects

of the density ratio ρ^*, the viscosity ratio η^* and Reynolds number on the wake length and, on the angle of separation are thoroughly investigated. The obtained results are important for the better understanding of processes in which droplets are rising or falling in an unbounded fluid.

THE PHYSICAL SYSTEM AND THE MATHEMATICAL FORMULATION

The period of droplet life during free rise or fall with a velocity u_∞ through a continuous phase is simulated in this work. For the purpose of the numerical simulation of the motion, a droplet fixed at a position in the stream of a flowing unbounded fluid is assumed. The flow configuration is illustrated in Figure 1. The flow at infinitely far away distance from the droplet is assumed uniform and its velocity is assumed equal to u_∞. The droplet is assumed spherical and has a constant diameter d_d, density ρ_d and viscosity η_d. The continuous phase has different fluid properties, i. e. different density ρ_c and viscosity η_c. The two phases are assumed immiscible or partly miscible with each other and both behave like Newtonian fluids. The flow in the continuous phase is communicated to the droplet through the interface as a result of which there is internal circulation inside the droplet. The following dimensionless relation holds for the system:

$$Re_c = Re_d \frac{\eta^*}{\rho^*},\qquad 1$$

where Re_c and Re_d respectively represent the Reynolds number in the continuous phase and in the droplet, η^* the ratio of droplet to the continuous phase viscosity, and ρ^* the ratio of droplet to the continuous phase density. The flow of the two-phase system can be fully described by the complete steady-state Navier-Stokes equations for the viscous, incompressible flow.

The two-phase flow problem being considered here is solved using the axisymmetric coordinates, which implies that the spherical drop reduces to a half circle in the (r, z) coordinates. This assumption is justified up to $Re_c = 300$ as discussed by Pruppacher et al. (1970). The physical system is thus best described by Navier-Stokes equations and the continuity equation for an incompressible viscous fluid in the cylindrical coordinates in two dimensions. The Navier-Stokes equations in this coordinate are:

$$\rho\left(u_r \frac{\partial u_r}{\partial r} + u_z \frac{\partial u_r}{\partial z} \right) = -\frac{\partial p}{\partial r} + \eta\left(\frac{\partial^2 u_r}{\partial r^2} + \frac{1}{r}\frac{\partial u_r}{\partial r} + \frac{\partial^2 u_r}{\partial z^2} - \frac{u_r}{r^2} \right)\qquad 2$$

and

$$\rho\left(u_r \frac{\partial u_z}{\partial r} + u_z \frac{\partial u_z}{\partial z} \right) = -\frac{\partial p}{\partial z} + \eta\left(\frac{\partial^2 u_z}{\partial r^2} + \right.$$

$$\left. \frac{1}{r}\frac{\partial u_z}{\partial r} + \frac{\partial^2 u_z}{\partial z^2} \right), \quad 3$$

and the continuity equation in the same coordinates is

$$\frac{1}{r}\frac{\partial}{\partial r}(ru_r) + \frac{\partial u_z}{\partial z} = 0. \quad 4$$

In the above equations, p and η represent the pressure and the fluid viscosity, u_r and u_z respectively the velocity in the r- und z-direction.

The numerical simulation of a flow problem required the prescription of the prevailing boundary conditions. These conditions for the case of a steady laminar flow of an incompressible Newtonian fluid past a liquid droplet are prescribed at an infinitely far distance from the droplet, at the droplet interface and at the symmetry line as follows: (i) The flow is assumed to be symmetric with respect to the z-axis. (ii) The interface between the droplet and the surrounding fluid is assumed smooth. The size of the droplet is constant and its shape is spherical. (iii) The velocity of fluid inside the droplet at $r = 0$ must remain finite, i.e. $u_r = 0$, $u_z \neq 0$. (iv) The tangential stresses at the interface between the two fluids must be equal. (v) The inflow velocity at sufficiently far distance from the droplet is uniform and is equal to u_r.

The steady flow of an isothermal fluid is fully described if the velocities, the pressure and all the fluid properties are known at every point of the flow field. In practice, the flow field is normally presented in a graphical form through streamlines, lines of constant value of stream functions, which are drawn such that they are tangential to the velocity vector at each point in a flow field. A stream of constant volume flow rate flows between two streamlines (Bird et al., 1960).

Solution Technique

In this work, the governing equations are solved, by using the finite element method. This method is a numerical analysis technique for obtaining approximate solutions to a wide variety of engineering problems. In this method, the flow field is divided into many small elements of convenient shapes and the unknown field variables are expressed in terms of assumed approximating (interpolation) functions within each element. The elements are connected together with one another through the nodes.

The solution of a partial differential equation through the finite element method is done by foremost casting the equation into an integral form. This is done by using either the variational method or the method of weighted residuals. The method of weighted residuals is the most convenient tool to transform the Navier-Stokes equations into integral form because the variational principles cannot be found for the equations. To apply the method of weighted residual for the solution of the Navier-Stokes equations, the velocities and pressure on each node of every element is approximated as follows

$$u_r = N \cdot u_r = \sum_{i=1}^{n} N_i u_{ri}, \quad 5$$

$$u_z = N \cdot u_z = \sum_{i=1}^{n} N_i u_{zi}, \quad 6$$

$$p = N \cdot p = \sum_{i=1}^{n} N_i^p p_i. \quad 7$$

The parameter N_i in the above equations denotes the interpolation function, n the number of nodes per element, and p, u_r and u_z respectively represent the pressure, the r- and the z- component of the velocity. Since the expressions in equations (5 - 7) only give an approximation of the actual values of the unknown for each node of every element, the substitution of these expressions in the Navier-Stokes and the continuity equations result in residuals or errors δ_i. These residuals are minimized or forced to vanish over the solution domain Ω by constructing an inner product (δ_i, W_i) between the residuals δ_i and the weighting functions W_i and setting this product equal to zero:

$$(\delta_i, W_i) = \int_{\Omega} \delta_i W_i d\Omega = 0. \quad 8$$

By the application of the Galerkin method, which is the most often used method to derive finite element equations in any problem involving fluid flow, the weighting functions are chosen to be the same as the interpolation function. The integration of the resulting expression over the element gives:

$$S^e u + N^e(u)u + L^{eT} p = F^e \quad 9$$

$$L^c u = 0 \quad 10$$

The symbol u denotes the discretised velocity vector, S^e the dissipation matrix, N^c the convective matrix, L^{eT} the pressure matrix, which is a transpose of the continuity matrix, and F^e the matrix containing the

boundary conditions. To reduce the number of equations that should be solved, the flow system was solved numerically together with the prescribed boundary conditions by using the penalty technique (Cuvelier et al., 1986). With this technique, the numerical simulation is greatly enhanced and thus, the computing time and the memory space required for computation are considerably reduced. The solution of the velocity field is obtained by the penalty technique through the expression:

$$S^e u + N^e(u)u + \frac{1}{\varepsilon}L^{e\top}M_p^{-1}L^e u = F^e \qquad 11$$

The parameter $1/\varepsilon$, depict the penalty parameter. The pressure p is obtained as a derivative of the velocity through the expression:

$$p = -\tau M_p^{-e1}L^e u . \qquad 12$$

The simulated area is discretised into many isoparametric triangular elements with each element having six nodal points. The matrices for all the elements were assembled and solved iteratively. A total of 5,693 isoparametric triangular elements were used in computation. This corresponds to a total of 11,552 nodal points out of which 4881 nodes were positioned in the drop. Equation 11 is a non linear equation. Its linearisation is done, by using Newton's iteration method. This method converges quadratically, but a good initial estimate is required which is obtained by solving the Stokes equations and next by iterating the equations through Picard's iteration method (Cuvelier et al., 1986).

RESULTS AND DISCUSSION

In order to validate and to demonstrate the accuracy of the present simulations, the computed flow fields are compared with existing results. This accuracy test is done by computing the drag coefficients of both solid spheres and liquid droplets, and comparing them with other results. The drag coefficient C_D of a solid sphere or spherical droplet is defined as follows:

$$C_D = \frac{F/A}{\rho_c u_\infty^2/2} . \qquad 13$$

The parameter A is the area of projection of the solid or liquid sphere and is given as $\pi d_d^2/2$, the product $\rho_c u_\infty^2/2$ is the dynamic pressure and F is the total force acting at the surface of a solid or liquid sphere.

The computed drag coefficients for solid sphere are compared with both the numerical and experimental data from Schlichting and Gersten (2000), and the numerical results from Tabata and Itakura (1995). The comparison is presented in Table 1. A close agreement between the present results and the other data can be seen in the table. The drag coefficients of liquid droplets with viscosity ratios $\eta^* = 1$ and $\eta^* = \infty$ are compared with both the data from Rivkind et al. (1976) and, Feng and Michaelides (2001) in Table 2. The results agree fairly well with both data, establishing that the results of the computations give a good presentation of the flow field. The variation of drag coefficient of liquid droplet with viscosity ratio for various value of Reynolds number, are presented in Table 3. The general trend of the results is that the drag coefficient decreases with increase in Reynolds number for a fixed viscosity ratio. For a particular Reynolds number, the drag coefficient increases with viscosity ratio.

The flow field is presented here in the form of stream function for easy visualisation. Figures 2a and 2b depict the stream function field for a Reynolds number of 100 and, a viscosity of 1 and 10 respectively. The figures show that both for $\eta^* = 1$ and $\eta^* = 10$, a well defined and simple recirculation flow occur in the droplets. The external flow is, however, a bit complex, being characterised by wake formation behind the droplets for $\eta^* = 10$. A comparison of the two flow fields suggests that viscosity ratio plays a significant roll on the flow inside and outside a sedimenting droplet.

Figure 3 presents the dependence of the critical Reynolds number (i. e. the Reynolds number at which wake first begins to form behind a droplet) on the viscosity ratio. It is seen that at a low viscosity ratio, a wake begins to form only at high Reynolds numbers. An increase in the viscosity ratio leads to the formation of the wake at lower Reynolds numbers. No wake was formed when the viscosity ratio is less than 2.3. This result established the conjecture of Wasowski and Blaß (1987) and Haas et al. (1972) that a wake can only form behind a bubble (a bubble is a droplet that has a viscosity ratio that is less than unity) if it is deformed and not when it has a spherical shape. The dynamics of a droplet without any wake formation is a consequence of unhindered impulse transfer through the interface of the droplet as compared with the one that exhibit some resistance to the transfer. The internal circulation of a droplet with a high viscosity ratio is greatly impeded by small impulse transfer through the interface.
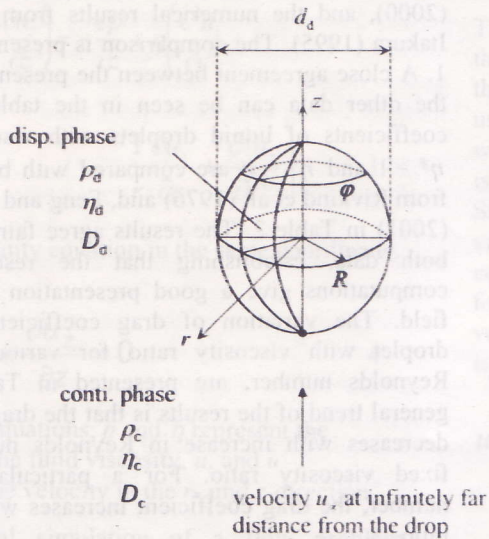
Figure 1: Schematic diagram of a liquid droplet sedimenting in a continuous fluid.
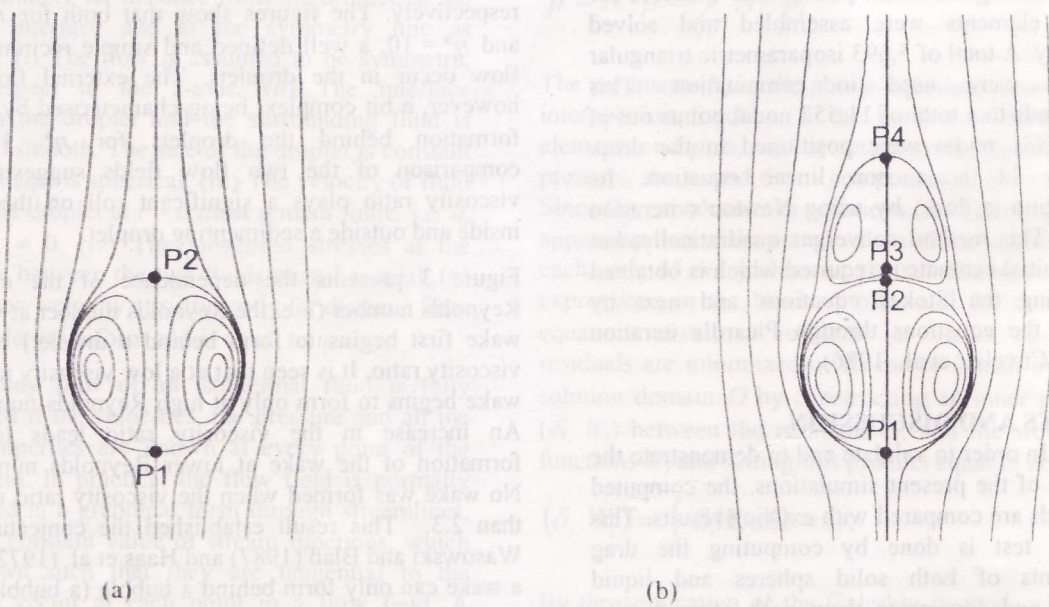

(a)   (b)

Figure 2: Flow field inside and outside a drop by $Re = 100$, $\rho^* = 1$ and (a) $\eta^* = 1$ and (b) $\eta^* = 10$.
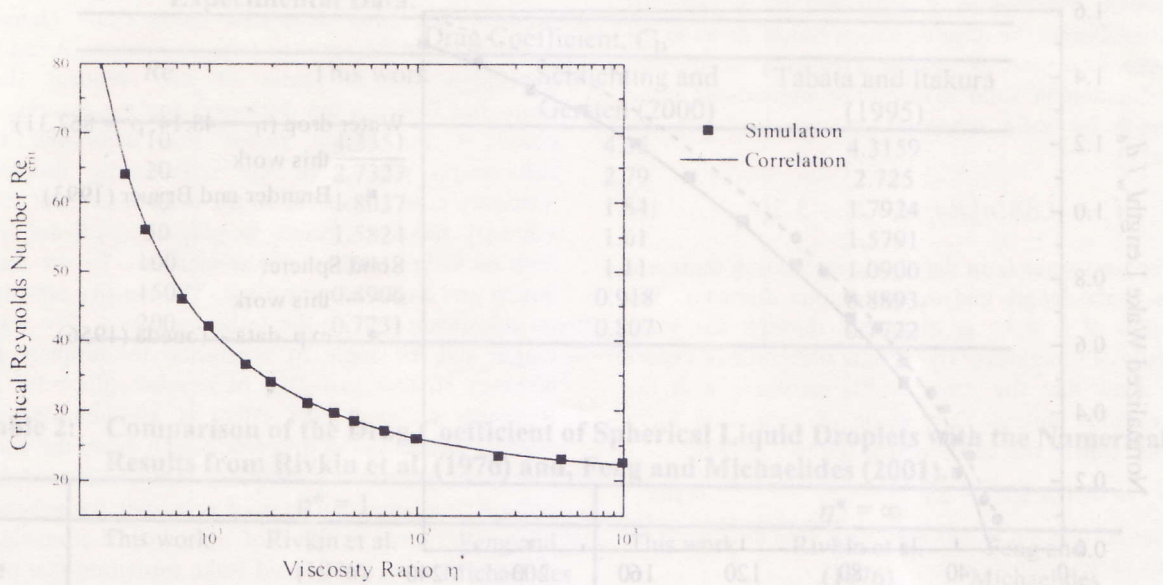
Figure 3: Critical Reynolds number for wake formation as a function of viscosity ratio for $\rho^* = 1$.

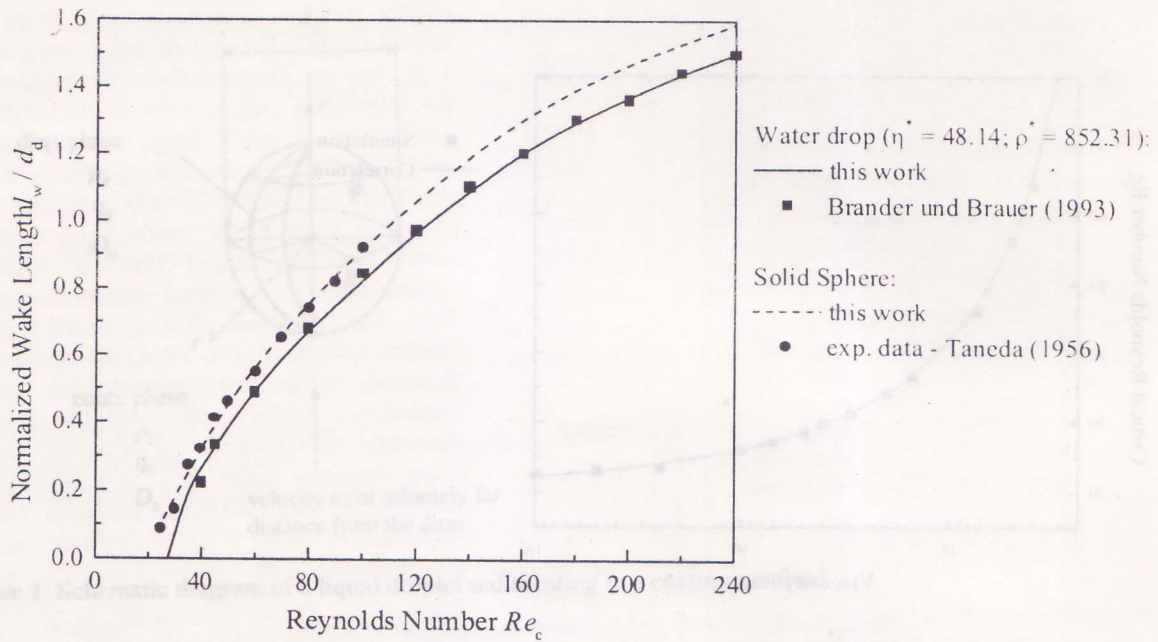Figure 4: The simulated streamlines around a solid sphere for $Re_c = 50$.

Figure 5: Comparison between the normalized wake length of solid sphere and that of water droplet.
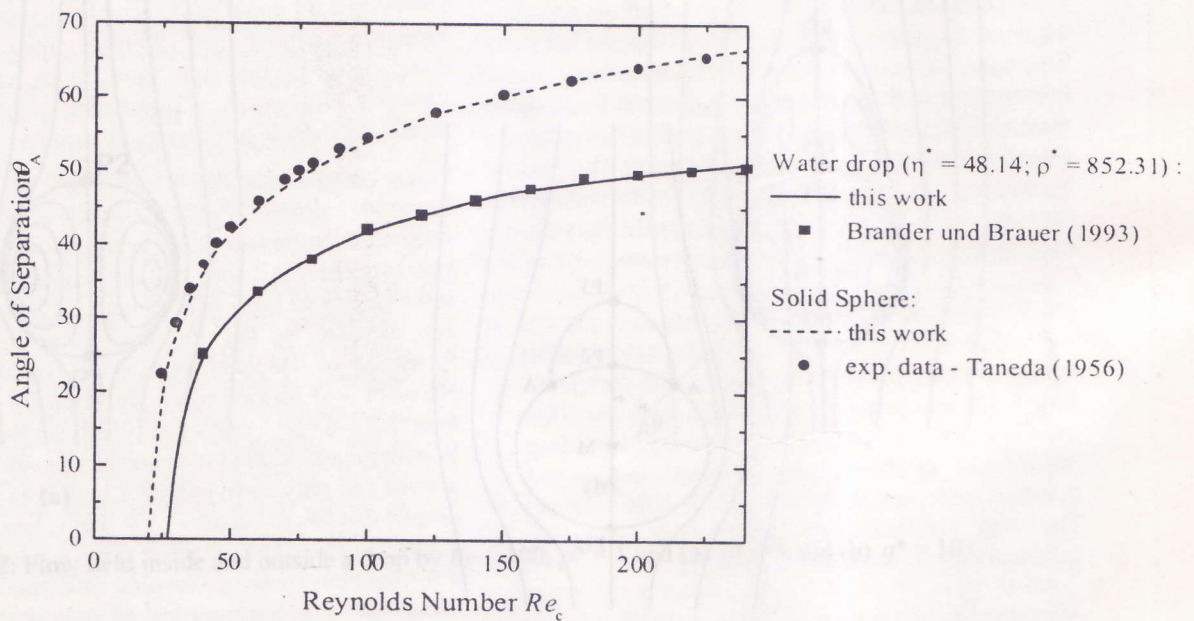

Figure 6: Comparison between the angle of separation for solid sphere and that of water droplet.

Table 1: **Comparison of the Drag Coefficient of Solid Sphere with Numerical and Experimental Data.**

Re	Drag Coefficient, C_D		
	This work	Schlichting and Gersten (2000)	Tabata and Itakura (1995)
10	4.3351	4.35	4.3159
20	2.7327	2.79	2.725
40	1.8037	1.84	1.7924
50	1.5824	1.61	1.5791
100	1.0918	1.11	1.0900
150	0.8906	0.918	0.8893
200	0.7731	0.807	0.7722

Table 2: **Comparison of the Drag Coefficient of Spherical Liquid Droplets with the Numerical Results from Rivkin et al. (1976) and, Feng and Michaelides (2001).**

Re	$\eta^* = 1$			$\eta^* = \infty$		
	This work	Rivkin et al. (1976)	Feng and Michaelides (2001)	This work	Rivkin et al. (1976)	Feng and Michaelides (2001)
1	22.3599	22.4	22.4	27.3153	27.4	27.3
10	3.3705	3.33	3.34	4.3599	4.28	4.30
20	2.0481	2.05	2.04	2.7434	2.71	2.71
50	1.0848	1.12	1.10	1.5864	1.58	1.56
100	0.6597	0.74	0.68	1.0939	1.11	1.10

The retarded internal circulation favour wake formation and development. The curve in Figure 3 shows that when the viscosity ratio tends to infinity, the critical Reynolds number tends to 20, which is in agreement with the critical Reynolds number of 20 for wake formation behind a solid sphere as determined through the extrapolation of the wake length to zero by Kalra and Uhlherr Kalra (1973), and by the numerical simulations of solid sphere by Pruppacher et al. (1970) and by Lin and Lee (1973). Further simulation results show that the density ratio plays no significant role on the wake formation. For example, wake is formed behind a droplet with fluid properties $\rho^* = 1$ and $\eta^* = 50$ and another droplet with fluid properties $\rho^* = 1000$ and $\eta^* = 50$ at the same Reynolds number $Re_c = 28.5$. But the critical Reynolds number for a droplet with $\rho^* = 1$ and $\eta^* = 5$ is 56. A correlation to predict the dependence of wake formation on the viscosity ratio is given below:

$$Re_{crit} = 52.1 \exp\left((\eta^* - 1.30)^{-0.5} - 31.6\right) \quad 14$$

This correlation is in close agreement with the results of the simulations when the density ratio is equals to unity

To establish the validity of the present results, the simulated results for the wake length and separation angle for solid sphere were compared with the known experimental results and correlation. Foremost, Figure 4 is used to define some standard notations as are used to describe wake. This Figure shows a simulated flow field around a solid sphere for a Reynolds number of 50. The point $P1$ and $P2$ in the Figure represent the front and the rear stagnation points on the droplet interface. The point A depicts the point at which the flow is separated from the droplet interface. This point occurs when the wall shear stress vanishes. The wake length is the distance between the points $P2$ and $P3$. The point $P3$ is a free stagnation point whose position is determined by the length of the wake. The angle of separation θ_A is defined as the angle between the lines $M\bar{A}$ and $M\bar{P}2$, where point M is the centre of the droplet.

The normalized wake length of a water droplet in air is presented in Figure 5 as a function of Reynolds number. The continuous curve is the results of the present computation and the square points are the results of Brander and Brauer (1993). A close agreement can be seen between the present results and that of Brander and Brauer. The curves show that the wake length increases with the Reynolds number. Brander and Brauer argued that the dynamics of a water droplet in air is similar to that of a solid sphere because of the wake formation behind the droplet. From Figure 5 a comparison between the wake length for solid sphere and water droplet can be made. It can

be seen that the wake length for a solid sphere is longer for any Reynolds number than that of water droplet. The reason is attributed to the internal circulation in the droplet, which causes delay in the wake formation as against a case of no internal circulation in solid sphere. The normalized wake length for solid sphere is correlated as (Brauer, 1979):

$$l_w/d_d = 0.88 ln(Re_c + 22) - 3.29 . \qquad 15$$

The parameter l_w in the above expression represent the wake length and d_d the droplet diameter. The width of a wake is measured through the wake angle of separation. The results presented in Figure 6 show that the wake width increases with the Reynolds number. The angle of separation for a solid sphere was correlated as (Brauer, 1979):

$$\theta_A = 44(ln\, Re_c - 3)^{0.45} \qquad (16)$$

This correlation agrees very well with the results of this present simulation.

The effect of viscosity ratio on the wake length and separation angle is gauged by plotting the wake length and the angle of separation over the viscosity ratio as a function of Reynolds number in Figures 7 and 8 respectively. These results are only valid for a droplet-continuous-phase system with the density ratio of unity. It can be seen that both the wake length and the angle of separation increase sharply with an increase in the viscosity ratio up to 15. There is no appreciable changes in the wake length and the angle of separation when the viscosity ratio is greater or equals to 20.

CONCLUSIONS

The flow characteristics of rising or falling droplets had been simulated using finite element method. From the results of the simulation, it can be concluded that the ratio of the identical fluid properties between the dispersed and the continuous phase is the major factor that determine the behavioural pattern of the sedimenting droplets. Viscosity ratio has effect on the drag coefficient. The viscosity ratio was found to play a significant role both on wake development as measured by the wake length and angle of separation. The density ratio has no significant role on the wake formation. The wake length and the angle of separation for droplets are however smaller than that of a solid sphere for all Reynolds number. This effect is attributed to the internal circulation in droplets, which delay the wake formation behind the droplets. The results of the present simulation can be used as a guide for selection of an operation velocity of any droplet-continuous phase system so as to avoid wake formation that may be detrimental to heat and mass transfer processes. The running cost of engineering equipment in which droplets occur, can thus be greatly reduced.

Table 3: **Variation of Drag Coefficient C_D of Liquid Droplet with Viscosity Ratio η^* for Various Value of Reynolds Number Re.**

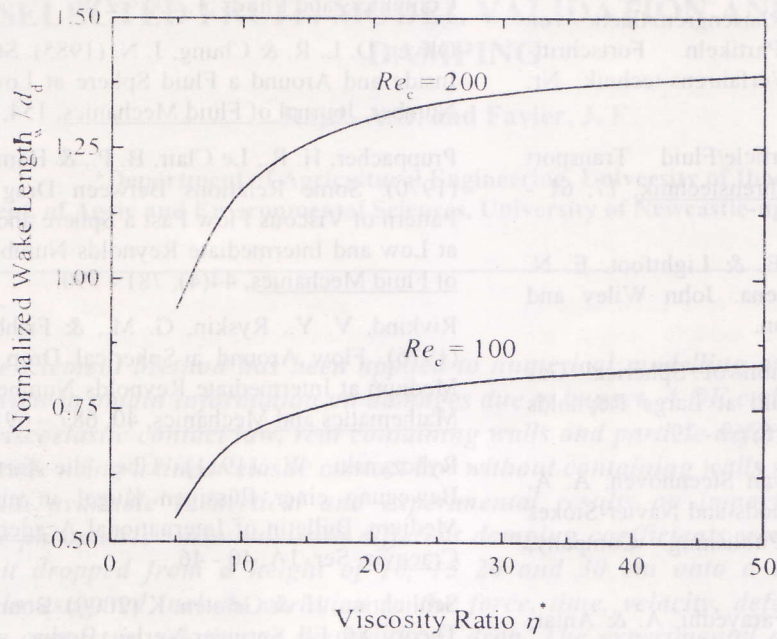|	Drag Coefficient, C_D			
Re	$\eta^* = 0.10$	$\eta^* = 5$	$\eta^* = 10$	$\eta^* = 20$
10	2.609380	4.02637	4.178440	4.265700
20	1.515380	2.51255	2.618460	2.678740
50	0.732412	1.42624	1.501270	1.542850
100	0.411400	0.957843	1,023390	1.058480
150	0.289611	0.762524	0.826317	0.859554
200	0.224452	0.647546	0.711227	0.754203
250	0.183644	0.568726	0.632698	0.664396
300	0.155608	0.509915	0.574232	0.605377

Figure 7: Dependence of the normalized wake length on the viscosity ratio for density ratio $\rho^* = 1$.

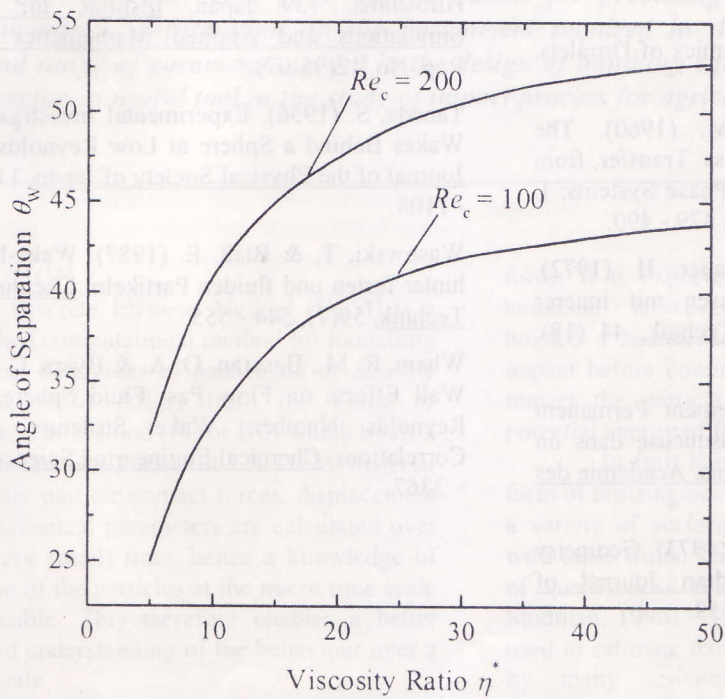Figure 8: Angle of separation in relation with the viscosity ratio for density ratio $\rho^* = 1$.

REFERENCES

Brander, B. & Brauer, H. (1993). Impuls- und Stofftransport durch die Phasengrenzfläche von kugelförmigen fluiden Partikeln. Fortschritt-Berichte VDI, Reihe 3: Verfahrens-technik, Nr. 326, VDI press, Düsseldorf.

Brauer, H. (1979). Particle/Fluid Transport Processes. Fortschritt-Verfahrenstechnik, 17, 61 - 99.

Bird, R. B., Stewart, W. E. & Lightfoot, E. N. (1960). Transport Phenomena. John Wiley and Sons Inc., New York, London.

Chao, B. T. (1962). Motion of Spherical Gas Bubbles in a Viscous Liquid at Large Reynolds Numbers. Physics of Fluids, 5, 69 - 79.

Cuvelier, C. Segal, A. & van Steenhoven, A. A. (1986). Finite Element Methods and Navier-Stokes Equations. D. Reidel Publishing Company, Dordrecht, Holland,

El-Shaarawi, M. A. I., Al-Farayedhi, A. & Antar, M. A. (1997). Boundary Layer Flow About and Inside a Liquid Sphere. Transactions of the ASME Journal of Fluids Engineering, 119, 42 – 49.

Feng, Z. & Michaelides, E. E. (2001). Drag Coefficients of Viscous Spheres at Intermediates and High Reynolds Numbers. Transactions of the ASME Journal of Fluids Engineering, 123, 841 – 849.

Frohn, A. Roth, N. (2000). Dynamics of Droplets. Springer-Verlag, Berlin.

Garner, F. H & Tayeban, M. (1960). The Importance of the Wake in Mass Transfer from Both Continuous and Dispersed Phase Systems: I. Anales de Física Y Química, 56B, 479 - 490.

Haas, U., Traub, H. S. & Brauer, H. (1972). Umströmung kugelförmiger Blasen mit innerer Zirkulation. Chemie Ingenieur Technik, 44 (18), 1060 - 1068.

Hadamard, J. S. (1911). Mouvement Permanent lent d'une Sphère Liquide et Visqueuse dans un Liquide Visqueux. Comptes Rendus, Academie des Sciences, 152, 1735 - 1743.

Kalra, T. R. & Uhlherr, P. H. T. (1973). Geometry of Bluff Body Wakes. Canadian Journal of Chemical Engineering, 51, 655 - 658.

Lin, C. L. & Lee, S. C. (1973). Transient State Analysis of Separated Flow Around a Sphere. Computers and Fluids, 1, 235 - 250.

Oliver, D. L. R. & Chung, J. N. (1985). Steady Flows Inside and Around a Fluid Sphere at Low Reynolds Number. Journal of Fluid Mechanics, 154, 215 - 230.

Pruppacher, H. R., Le Clair, B. P., & Hamielec, A. E. (1970). Some Relations Between Drag and Flow Pattern of Viscous Flow Past a Sphere and a Cylinder at Low and Intermediate Reynolds Numbers. Journal of Fluid Mechanics, 44(4), 781 - 790.

Rivkind, V. Y., Ryskin, G. M., & Fishbein, G. A. (1976). Flow Around a Spherical Drop in a Fluid Medium at Intermediate Reynolds Numbers. Applied Mathematics and Mechanics, 40, 687 – 691.

Rybczynski, W. (1911). Über die fortschreitende Bewegung einer flüssigen Kugel in einem zähen Medium. Bulletin of International Academic Science Cracovia, Ser. 1A, 40 - 46.

Schlichting, H. & Gersten, K (2000). Boundary-Layer Theory. 8th Ed. Springer-Verlag, Berlin.

Sirignanoi, W. A. (1993). Fluid Dynamics of Sprays – 1992 Freeman Scholar Lecture. Transactions of the ASME Journal of Fluids Engineering, 115, 345 - 378.

Tabata, M. & Itakura, K. (1995). Precise Computation of Drag Coefficients of the Sphere; Department of Mathematics, Hiroshima University, Higashi-Hiroshima, 739 Japan, Institute for Numerical Simulations and Applied Mathematics (INSAM), Rep. No. 12(95-07).

Taneda, S. (1956). Experimental Investigation of the Wakes Behind a Sphere at Low Reynolds Numbers. Journal of the Physical Society of Japan, 11(10), 1104 - 1108.

Wasowski, T. & Blaß, E. (1987). Wake-Phänomene hinter festen und fluiden Partikeln. Chemie Ingenieur Technik, 59(7), 544 - 555.

Wham, R. M., Basaran, O. A. & Byers, C. H. (1997). Wall Effects on Flow Past Fluid Spheres at Finite Reynolds Number: Wake Structure and Drag Correlations. Chemical Engineering Science, 52, 3345 – 3367.